Double Scattering in Deuteron Electrodisintegration

Werner U Boeglin and Misak M Sargsian

Florida International University, Miami, FL 33199

(Dated: February 22, 2024)

We demonstrate that at sufficiently high energies where the eikonal regime is established for hadronic interactions, the double scattering subprocess can be clearly identified and isolated in quasi-elastic deuteron electro-disintegration processes. Comparing theoretical calculations with the recent high precision experimental data we present a "proof of principle" that these processes can be used to study advanced issues related to hadron formation in QCD. In this case, the double scattering represents as a fermi-scale "detector" which probes products of high Q^2 scattering from the bound nucleon through their rescattering from the spectator nucleon in the deuteron.

I. INTRODUCTION

One of the important topics in the exploration of the quantum chromodynamic (QCD) structure of hadrons is understanding their formation from quark-gluon systems, the role of the confinement and color field distribution inside hadrons. The main approach in studying these properties is to consider hadron production processes involving nuclei where the nuclear medium is used as a "detector" in kind, in probing interaction dynamics related to the discussed above phenomena.

One of the best known examples of this strategy is the heavy-ion collision[1, 2] in pursuing the detection of quark-gluon plasma or probing hadronization in deep-inelastic processes in AA, pA (see e.g. [3–5]) and eA (see e.g. [6, 7]) scatterings. Studies of heavy ion and pA scattering processes have been carried out for many decades resulting in a significant progress in understanding of many aspects of QCD dynamics of hadron formation. However the progress was made only in those instances in which the precise knowledge of nuclear structure to interpret the data was not essential. This is associated with the complication of accounting for nuclear effects in case of medium and heavy nuclei.

In this work we demonstrate that the most simple nucleus, the deuteron, can be used to perform some of the explorations of QCD dynamics of baryons. The advantage in this case is that one can calculate the nuclear effects with sufficiently high accuracy. The idea that the deuteron can be used to probe QCD dynamics of hard processes by focusing on the rescattering (or double scattering) subprocess in high Q^2 deuteron electrodisintegration, was suggested in the 1990s [8–10]. The idea was do use the energy dependence of double scattering strength as a test for the onset of color transparency (CT) phenomena. Very recently a dedicated experiment[11] has been approved by the Program Advisory Committee of Jefferson Lab which will probe the onset of CT for double scattering processes for up to $Q^2 = 14$ (GeV/c)^2.

However the concept that double scattering can be clearly isolated and is sensitive to the energy dependence of the amplitude of pn-scattering was never proven experimentally for a benchmark measurement in which one expects the dominance of the hadronic picture in the rescattering (i.e. no CT effects). To prove this concept as a baseline for probing novel QCD effects one needs Q^2 large enough that it would be possible to clearly isolate the (double scattering) process in which the produced nucleon in the $\gamma^* N$ interaction in the deuteron re-scatters off the spectator nucleon. On the other hand Q^2 needs to be moderate enough that the hadronic picture of rescatteirng is valid and no CT effects are expected. Once such a subprocess and its energy sensitivity to pn-scattering is established, one can extend these studies to higher Q^2 to explore the onset of hard QCD dynamics.

In view of such a program, only recently the first high accuracy measurements at moderately high Q^2 became available that the above mentioned concept could be verified.

In this work we use recent progress in both theoretical and experimental studies of deuteron electrodisintegration processes in $Q^2 \sim few$ (GeV/c)^2 kinematics to check; (I) if the double scattering subprocess can be isolated and described and (II) if the energy dependence of pn rescattering, in which the one (fast) nucleon is produced by the $\gamma^* N$ interaction off the bound nucleon and the other nucleon is the spectator in the deuteron, reflects the energy dependence of the free pn-scattering amplitude known independently from $pn \to pn$ elastic scattering experiments.

In Section II we discuss briefly the theory of high Q^2 electrodisintegration of the deuteron. Then in Sec. III we focus on kinematics maximally sensitive to the double scattering subprocess and investigate the sensitivity of the electro-disintegration reaction in this case to the amplitude of high energy pn scattering. In Section IV we present the discussion of the recent experiments of deuteron electro-disintegration at moderately large Q^2 performed at Jefferson Lab, focusing again on double scattering kinematics. In section V we present the comparison of theory with experiment in double scattering kinematics and demonstrate that the available data already show the sensitivity of the cross section to the energy dependence of the proton-neutron scattering amplitude thus providing a proof of the principle of isolating and probing the subprocess of high energy pn rescattering in the deuteron. In Sec.VI we present conclusions and discuss how these types of processes can be used
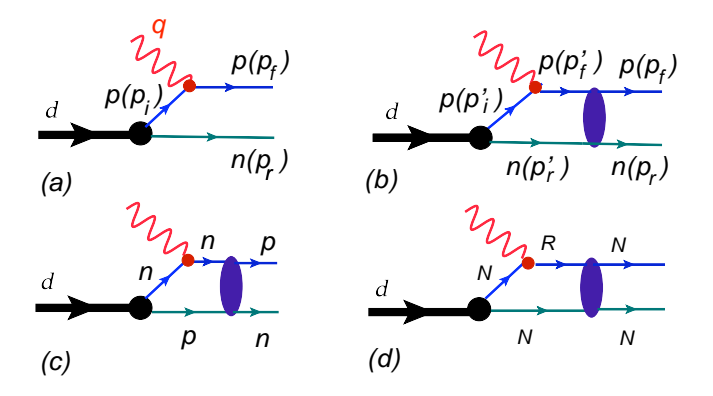
FIG. 1. Diagrams of electrodisintegration amplitude.

in studies of color transparency as well as hadronization processes in the high Q^2 limit.

II. HIGH Q^2 ELECTRO-DISINTEGRATION OF THE DEUTERON IN GENERALIZED EIKONAL APPROXIMATION

We are discussing the process of exclusive deuteron electro-disintegration:

$$e + d \rightarrow e' + N_f + N_r, \tag{1}$$

at large four-momentum transfer, $Q^2 \equiv \mathbf{q}^2 - q_0^2$, kinematics, where $\mathbf{q}$ and q_0 are three-momentum and energy of virtual photon. We assign to the struck (N_f) and recoil (N_r) nucleons four-momenta $(E_f, \mathbf{p_f})$ and $(E_r, \mathbf{p_r})$ respectively. For specificity we also consider the struck nucleon to be a proton and the recoil a neutron. One also introduces the missing momentum as; $\mathbf{p_m} \equiv \mathbf{q} - \mathbf{p_f}$ Note that for the considered reaction, $\mathbf{p_m} = \mathbf{p_r}$.

The kinematics are such that one can clearly identify the struck nucleon from the recoil nucleon with $p_f \sim q \gg p_r \sim m_N$. The latter, together with the requirement, $Q^2 \gg m_N^2$ provides a high energy condition for the process in which one can treat $\frac{q_0 - q_z}{q_0 + q} \ll 1$ and $\frac{E_f - p_{f,z}}{E_f + p_{f,z}} \ll 1$ as small parameters. The emergence of such small parameters allows one to prove the reduction theorem[12] in which case all possible final state interactions (FSI) of outgoing nucleons are ordered in such a way that they can be summed up into the single off-shell phenomenological pn scattering amplitude. This makes it possible to formulate an effective Feynman diagrammatic rules[12], using which allows one to perform calculations in a self-consistent way taking into account the relativistic kinematics of the scattering process.

The above discussed theoretical simplifications created a new opportunity for investigating reaction(1) in the high energy limit resulting in intensive theoretical efforts to calculate these processes considering also polarization degrees of freedom (see. e.g. Refs. [13–17]).

In the discussed high energy limit it can be shown[17, 18] that only four diagrams contribute to the process of Eq.(1), representing plane wave impulse approximation (PWIA)(Fig.1(a)), contribution with final state $pn \rightarrow pn$ rescattering (FSI) (Fig.1(b)), contribution with charge interchange $pn \rightarrow np$ rescattering (ChEx-FSI),(Fig.1(c)) and with $RN \rightarrow pn$ rescattering (Fig.1(d)) in which R represents the resonance produced from electron scattering off the bound nucleon. Other contributions including meson-exchange currents, and spectator production in which nucleon N_f is the recoil rather than the struck nucleon are parametrically small. We represent the four dimensional scattering amplitude A^μ through the sum of the above contributions as follows:

$$\langle s_f, s_r \mid A^\mu \mid s_d \rangle = \langle s_f, s_r \mid A_0^\mu \mid s_d \rangle + \langle s_f, s_r \mid A_1^\mu \mid s_d \rangle$$
$$+ \langle s_f, s_r \mid A_{1,chex}^\mu \mid s_d \rangle + \langle s_f, s_r \mid A_{1,R}^\mu \mid s_d \rangle, \tag{2}$$

where s_d, s_r and s_f represent the spin states of the initial deuteron, the final recoil and the struck nucleon, respectively. The amplitudes A_0, A_1, $A_{1,chex}$ and $A_{1,R}$ correspond to the diagrams of PWIA, single diagonal, charge-interchange and $RN \rightarrow NN$ rescattering contributions.

With the scattering amplitude defined this way the unpolorized differential cross section for the process (1) can be written as follows:

$$\frac{d\sigma}{dE_e', d\Omega_{e'} dp_f d\Omega_f} =$$
$$\frac{\alpha^2 E_e'}{q^4 E_e} \cdot \frac{1}{6} \sum_{s_f, s_r, s_d, s_1, s_2} \frac{\mid J_e^\mu J_{d,\mu} \mid^2}{2 M_d E_f} \frac{p_f^2}{\mid \frac{p_f}{E_f} + \frac{p_f - q\cos(\theta_{p_f,q})}{E_r} \mid} \tag{3}$$

where E_e and E_e' are energies of the incoming and scattered electrons, and M_d is the mass of the deuteron. Here the leptonic current is defined as $J_e^\mu = \bar{u}(k_2, s_2)\gamma^\mu u(k_1, s_1)$, with $u(k, s)$ being the Dirac bispinors. The electromagnetic transition current of the deuteron is defined as

$$J_d^\mu = \frac{\langle s_f, s_r \mid A^\mu \mid s_d \rangle}{\sqrt{2(2\pi)^3 2 E_r}}, \tag{4}$$

where $\langle s_f, s_r \mid A^\mu \mid s_d \rangle$ presented in Eq.(2).

Further simplification is achieved if one chose the kinematics away from the threshold of resonance, R production. In this case only PWIA and FSI and CHEX-FSI contributions define the cross section of the deuteron electrodisintgration.

A. PWIA Contribution

In the calculation of the PWIA term for not extremely large internal momenta of the deuteron $p_i \leq 600$ MeV/c, in which case Z-graph contributions are small correction the virtual nucleon approximation is justified[17]. Within the effective Feynman diagrammatic approach[12] one

uses diagrammatic rules to obtain:

$$\langle s_f, s_r \mid A_0^\mu \mid s_d \rangle =$$
$$-\bar{u}(p_r, s_r)\Gamma_{\gamma^* p}^\mu \frac{\not{p}_i + m}{p_i^2 - m^2} \cdot \bar{u}(p_f, s_f)\Gamma_{DNN} \cdot \chi^{s_d}, \quad (5)$$

where $\Gamma_{\gamma^* p}$ is the electromagnetic vertex of the $\gamma^* N \to N$ scattering and the vertex function Γ_{DNN} describes the transition of the deuteron into the pn system. Then projecting the deuteron transition vertex to the positive energy solution of the bound nucleon propagator and considering the spectator nucleon as on-shell, one introduces the deuteron wave function[19, 20] in the form:

$$\Psi_d^{s_d}(s_i, p_i, s_r, p_r) = -\frac{\bar{u}(p_i, s_i)\bar{u}(p_r, s_r)\Gamma_{DNN}^{s_d}\chi_{s_d}}{(p_i^2 - m^2)\sqrt{2}\sqrt{(2\pi)^3(p_r^2 + m^2)^{\frac{1}{2}}}}, \quad (6)$$

in which the bound nucleon is off-energy shell with $E_i^{off} = M_d - \sqrt{m_N^2 + p_r^2}$ and initial momentum $\mathbf{p_i} = -\mathbf{p_m}$. To treat the off-shellness of the bound nucleon in the $\gamma^* N$ scattering one splits the initial nucleon propagator into on- and off-shell parts that yield on- and off- shell components of the electromagnetic current for interaction with the incoming electron (for details see Ref.[17]). This results in:

$$\langle s_f, s_r \mid A_0^\mu \mid s_d \rangle = \sqrt{2}\sqrt{(2\pi)^3 2E_r} \times$$
$$\sum_{s_i} J_N^\mu(s_f, p_f; s_i, p_i)\Psi_d^{s_d}(s_i, p_i, s_r, p_r), \quad (7)$$

where

$$J_N^\mu(s_f, p_f; s_i, p_i) =$$
$$J_{N,on}^\mu(s_f, p_f; s_i, p_i) + J_{N,off}^\mu(s_f, p_f; s_i, p_i) \quad (8)$$

in which on- and off- shell components of electromagnetic current of the bound nucleon are defined as follows:

$$J_{N,on}^\mu(s_f, p_f; s_i, p_i) = \bar{u}(p_f, s_f)\Gamma_{\gamma^* N}^\mu u(p_i, s_i)$$
$$J_{N,off}^\mu(s_f, p_f; s_i, p_i) = \bar{u}(p_f, s_f)\Gamma_{\gamma^* N}^\mu \gamma^0 u(p_i, s_i) \times$$
$$\frac{E_i^{off} - E_i^{on}}{2m}, \quad (9)$$

with the electromagnetic vertex expressed through two independent Dirac and Pauli form-factors:

$$\Gamma^\mu = F_1(Q^2)\gamma^\mu + \frac{F_2(Q^2)}{2m}i\sigma^{\mu,\nu}q_\nu. \quad (10)$$

B. FSI Contribution

The FSI and ChEx-FSI diagrams in Fig.1(b) and (c) are calculated within the Generalized Eikonal Approximation[12, 17, 21] in which using effective Feynman diagrammatic rules[12] one calculates the scattering amplitude as:

$$\langle s_f, s_r \mid A_1^\mu \mid s_d \rangle = -\int \frac{d^4 p_r'}{i(2\pi)^4}$$
$$\times \frac{\bar{u}(p_f, s_f)\bar{u}(p_r, s_r)F_{NN}[\not{p}_r' + m][\not{p}_d - \not{p}_r' + \not{q} + m]}{(p_d - p_r' + q)^2 - m^2 + i\epsilon}$$
$$\times \frac{\Gamma_{\gamma^* N}[\not{p}_d - \not{p}_r' + m]\Gamma_{DNN}\chi^{s_d}}{((p_d - p_r')^2 - m^2 + i\epsilon)(p_r'^2 - m^2 + i\epsilon)}, \quad (11)$$

were F_{NN} represents the invariant off-shell direct $pn \to pn$ or charge-interchange $pn \to np$ scattering amplitude, that can be expressed as follows:

$$F_{NN}(s, t) = \sqrt{s(s - 4m^2)}f_{NN}(s, t), \quad (12)$$

with $s = (q + p_d)^2 = (p_f + p_r)^2$ and $t = (p_r' - p_r)^2$. Here f_{NN} represents the parametrization of the pn direct and charge-exchange scattering amplitudes in the diffractive form such that for direct scattering $Im f_{NN} = \sigma_{pn}^{tot}$, where σ_{pn}^{tot} is the total pn scattering cross section.

Furthermore, in Eq.(11) we first, integrate by $d^0 p_{r'}$ through the positive energy pole of the spectator nucleon in the intermediate state, then integrate by $p_{r,z}'$ splitting the propagator of the struck nucleon in the intermediate state into pole and principal-value parts. This results in:

$$\langle s_f, s_r \mid A_1^{\mu} \mid s_d \rangle = \frac{i\sqrt{2}(2\pi)^{\frac{3}{2}}}{4} \sum_{s_f', s_r', s_i} \int \frac{d^2 p_r'}{(2\pi)^2} \frac{\sqrt{2\tilde{E}_r'}\sqrt{s(s-4m^2)}}{2\tilde{E}_r'|q|} \langle p_f, s_f; p_r, s_r \mid f^{NN,on}(t,s) \mid \tilde{p}_r', s_r'; \tilde{p}_f', s_f' \rangle$$

$$\times J_N^{\mu}(s_f', p_f'; s_i, \tilde{p}_i') \cdot \Psi_d^{s_d}(s_i, \tilde{p}_i', s_r', \tilde{p}_r')$$

$$-\frac{\sqrt{2}(2\pi)^{\frac{3}{2}}}{2} \sum_{s_f', s_r', s_i} \mathcal{P} \int \frac{dp_{r,z}'}{2\pi} \int \frac{d^2 p_r'}{(2\pi)^2} \frac{\sqrt{2E_r'}\sqrt{s(s-4m^2)}}{2E_r'|\mathbf{q}|} \frac{\langle p_f, s_f; p_r, s_r \mid f^{NN,off}(t,s) \mid p_r', s_r'; p_f', s_f' \rangle}{p_{r,z}' - \tilde{p}_{r,z}'}$$

$$\times J_N^{\mu}(s_f', p_f'; s_i, p_i') \cdot \Psi_d^{s_d}(s_i, p_i', s_r', p_r'), \tag{13}$$

where $\tilde{p}_r' = (p_{r,z} - \Delta, p_{r,\perp}')$, $\tilde{E}_r' = \sqrt{m^2 + \tilde{p}_r'^2}$, $\tilde{p}_i' = p_d - \tilde{p}_r'$ and $\tilde{p}_f' = \tilde{p}_i' + q$ and

$$\Delta = \frac{q_0}{|\mathbf{q}|}(E_r - E_r') + \frac{M_d}{|\mathbf{q}|}(E_r - E_r') + \frac{p_r'^2 - m^2}{2|\mathbf{q}|}. \tag{14}$$

Note that while $f^{NN,on}(t,s)$ is taken from experiments the off-shell counterpart is modeled according to the relation:

$$f^{NN,off} = f^{NN,on}e^{B(m_{off}^2 - m^2)}, \tag{15}$$

where $m_{off}^2 \equiv (p_f')^2$. As it follows from Eq.(13) the principal value part of FSI contributes to the real part of the rescattering amplitude which is small in high energy limit. As a result the accuracy of the approximation in Eq.(15) is not expected to render large uncertainities in the overall estimate of the rescattering contribution.

Regarding the $f^{NN,on}$ amplitude one obtains it from the analysis of experiments in direct $pn \rightarrow pn$ scattering for evaluating FSI and $pn \rightarrow np$ scattering for evaluating ChEx-FSI. It is worth mentioning that $pn \rightarrow np$ scattering is dominated by pion exchange. As a result its amplitude decreases with increasing energy by a factor of $\sqrt{s}$ compared to the direct $pn \rightarrow pn$ scattering. The latter, at considered energies, in forward direction is dominated by Pomeron exchange with a weak energy dependence and is predominantly imaginary. Thus, the pole term in Eq.(13) has a dominating contribution from the direct $pn \rightarrow pn$ scattering amplitude

III. DOUBLE SCATTERING CONTRIBUTION

The total invariant energy of the reaction (1) is defined as

$$s \equiv (q + p_d)^2 = M_d^2 + Q^2(\frac{M_d}{m_N x} - 1), \tag{16}$$

which indicates that it linearly grows with Q^2. For sufficiently large s one expects that the direct FSI amplitude defines the whole dynamics of the final state interaction in the reaction (1). In this case the FSI amplitude can be parameterized as:

$$f_{pn}(s,t) = (\sigma_{pn,tot}(s)(i + \alpha(s))e^{-\frac{B(s)}{2}t}, \tag{17}$$

where the real part of the amplitude $\alpha(s)$ is a small correction in the high energy limit. The total pn scattering cross section is defined by $\sigma_{pn,tot}(s)$. These and other parameters $\alpha(s)$ and $B(s)$ are defined from the $pn \rightarrow pn$ scattering experiments. The comparison of the fit of $\sigma_{pn,tot}$ with available data[22] is shown in Fig.2 which indicates noticeable dependence on the invariant energy up to $s \leq 20$ GeV^2, the range within which current experiments of reaction (1) are performed.
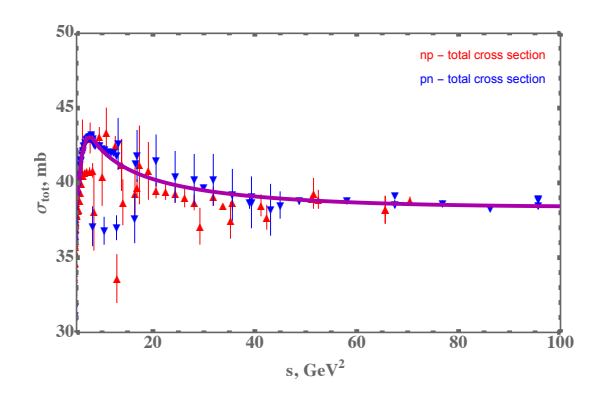

FIG. 2. Comparison of the parametrization of $\sigma_{pn,tot}$ with the experimental data [22] as a function of s.

Because of the predominantly imaginary nature of the f_{pn} amplitude the cross section of the reaction (1) is proportional to the following combination of the scattering amplitudes:

$$\mid A \mid^2 = \mid A_{PWIA} \mid^2 - 2\mathcal{R}e A_{PWIA} A_{FSI} + \mid A_{FSI} \mid^2. \tag{18}$$

Here with the increase of missing momentum in the reaction A_{PWIA} decreases much faster than A_{FSI}, since for the former the wave function is defined by the magnitude of the recoil momentum p_r while for the latter it is an integral in Eq.(13) which is dominated at smaller values of momenta entering the wave function of the deuteron. As a result if we construct a ratio:

$$R_{PWIA} = \frac{\sigma_{Full}}{\sigma_{PWIA}}, \tag{19}$$

where σ_{PWIA} is the cross section (3) calculated by PWIA amplitude only and σ_{Full} includes also rescattering amplitudes, then at small p_r the ratio is close to unity; then it decreases with an increase of p_r due to the increasing

contribution of the interference term in Eq.(18). However, with the further increase of p_r, the dominating term becomes the term proportional to $\mid A_{FSI} \mid^2$ (hereafter referred to *double scattering term*). This dominance reflects the fact that the interference term is proportional to the deuteron wave function with the argument of p_r while the double scattering term is defined only by the integral (13), in which deuteron momentum is integrated over the transverse component of the momentum transfer in the rescattering. As a result, the further increase of p_r will result in the diminishing interference term, while the $\mid A_{FSI} \mid^2$ changes slowly. Thus one expects strong dependence of the ratio R as a function of p_r in the kinematics dominated by final state reinteractions. This pattern for R is predicted in Refs.[12, 17, 21] presented in Fig.3. As one can see in the figure the FSI is large at
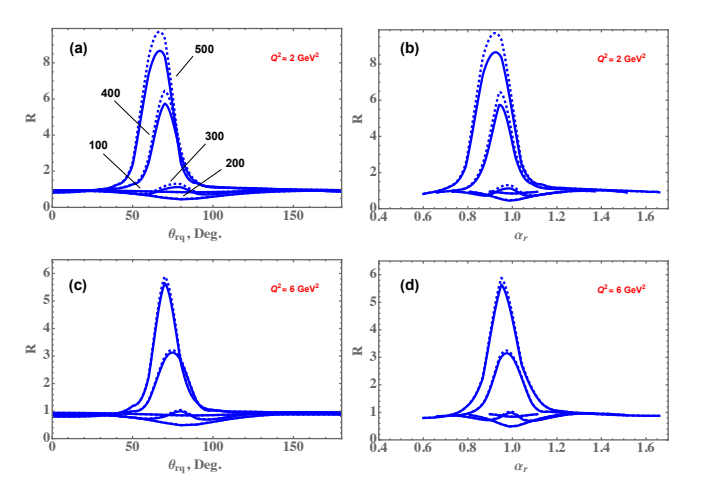

FIG. 3. The dependence of R on the angle of recoil nucleon for different values of recoil momenta (a) and (c) or different values of light-front momentum fraction of recoil nucleon (b) and (d). Solid curves corresponds to calculations that include PWIA and FSI terms, while dashed line include also ChEx-FSI.

transverse angles $\theta_{rq} \sim 70^\circ - 80^\circ$ with the double scattering term dominating at $p_r \gtrsim 400$ MeV/c at $\theta_r \approx 70^0$. The latter corresponds to the situation in which the momentum entering in the wave function in the integrand of the pole part of Eq.(13) is very small, maximizing the FSI amplitude. In many cases, it is convenient to consider the FSI contribution as a function of the light cone momentum fraction of the deuteron carried by the recoil nucleon: $\alpha_r = \frac{E_r - p_{r,z}}{m_N}$. The choice of α_r as a kinematic parameter is associated with the fact that it provides a Lorentz boost invariant condition for maximal FSI effect at $\alpha_r \approx 0.9 - 1$ (see Fig.3(b)(d)).

If the cross section of reaction (1) at above discussed kinematics ($p_r \geq 400$ MeV/c and $\alpha_r \approx 0.9 - 1$) is defined predominantly by the double scattering term and the all above mentioned effects, like principal value and charge-interchange FSI contributions are small at high energy, then one expects that the s-dependence of the ratio R (19) should reflect the s dependence of $\mid f_{pn}(s,t) \mid^2$
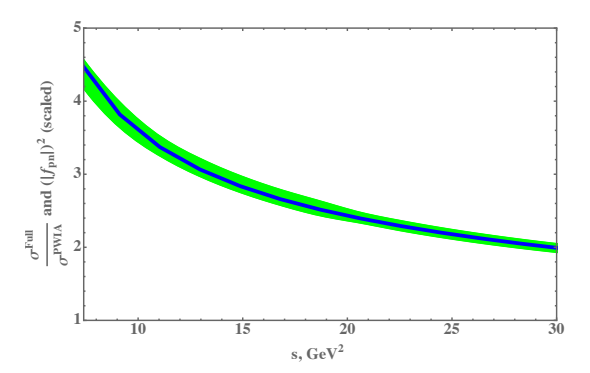
defined in Eq.(17). To verify this, in Fig.4 we compare

FIG. 4. Comparison of double scattering contribution to the $\mid f_{pn}(s,t) \mid^2$.

the s dependencies of ratio-R and $\mid f_{pn}(s,t) \mid^2$ (scaled at $s = 30$ GeV^2) for $\alpha_r = 1$ and $p_r = 400$ MeV/c and $\phi_{rq} = \pi$. As the figure shows the double scattering term reproduces the shape of the energy dependence of the modulus square of the pn scattering amplitude very well. This comparison shows that the cross section of reaction (1) at the kinematics of double scattering can be used as a tool for investigation of the energy dependence of the amplitude of pn elastic scattering in high energy limit. This is the main argument for the reaction (1) to be used for investigation of the hadronic interactions in the deuteron at much larger Q^2.

IV. EXPERIMENTAL STATUS OF HIGH Q^2 ELECTRO-DISINTEGRATION PROCESSES IN DOUBLE SCATTERING KINEMATICS

Early experiments of reaction (1) carried out with electron accelerators with energies below 1 GeV were able to measure coincidence cross sections at large missing momenta, however, these measurements were dominated by long range processes that prevented one to probe the short range structure of the deuteron (for a discussion and summary of low energy experiments see Ref. [18] and references therein). In these experiments due to the relatively low incident energy and the associated low momentum transfer it was not possible for example, to separate an event where a large initial momentum proton was hit and the spectator neutron recoiled with the equal and opposite momentum from an event where a lower momentum neutron was hit and the recoiling proton was measured. The second contribution can become important when the final state proton momentum is of the same order or even smaller than the missing momentum being probed. This situation changed with the operation of Jefferson Lab which allowed experiments using the 6 as well as the 11 GeV high intensity continuous wave

electron beams. In these experiments final state proton momenta were typically more than 1.5 GeV/c which is about a factor three larger than the largest missing

momenta probed.

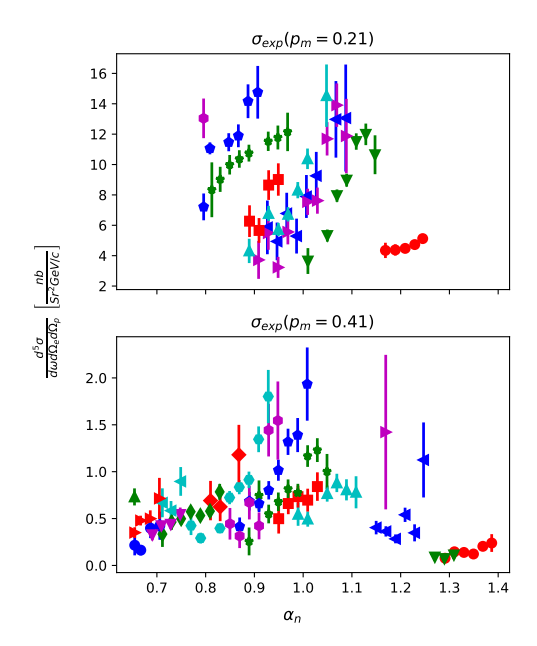FIG. 5. Experimental cross sections as a function of α_n for $Q^2 = 2.1$ (GeV/c)^2. Top panel $p_m = 0.21$ GeV/c, bottom panel $p_m = 0.41$ GeV/c. The different color and symbol combinations correspond to the different contributing spectrometer settings.

Experiments carried out in Hall A [23] and at CLAS in Hall B [24] of Jefferson Lab, measuring D(e,e'p)n cross sections for missing momenta up to 0.5 GeV/c over a range of neutron recoil angles from $\sim 10°$ up to almost 180° with momentum transfers being order of *several* (GeV/c)^2. Especially the Hall A experiment with its fine kinematic binning allowed one to perform a detailed study of the D(e,e'p)n reaction for different, well-defined kinematic settings. Missing momentum distributions for the high momentum transfer data-set ($Q^2 = 3.5$ (GeV/c)^2) have been published[23] together with recoil angular distributions of the neutron for missing momenta of $p_m = 0.2, 0.4$ and 0.5 GeV/c. Both, Hall A and Hall B experiments demonstrated that at $Q^2 \gtrsim 2$ (GeV/c)^2 FSI are strongly anisotropic in the angle of the recoil neutron (θ_{nq}) with respect the 3-momentum transfer, **q** peaking at $\theta_{nq} \sim 70°$ and being small at parallel and antiparallel directions. It is worth mentioning that at lower Q^2 ($Q^2 = 0.8$ (GeV/c)^2) large FSI contributions were found for all recoil angles for missing momenta of 0.4 GeV/c and above [25].

As it was discussed in Sec. III, the above mentioned anisotropy of FSI is the signature of the onset of the high energy regime and was predicted by eikonal based models such as the generalized eikonal approximation [8, 12, 21] as well as models based on similar high energy approximations[13–17].

This anisotropy made it possible to select kinematic regions where FSI are reduced, providing a more direct

access to the underlying momentum distribution in the deuteron. Probing a "genuine" momentum distribution in the deuteron by selecting kinematics of reduced FSI was the goal of the first measurement[23] as well as a recent measurement at larger $Q^2 = 4.25$(GeV/c)^2 and at significantly larger missing momenta, up to 1 GeV/c. It is worth mentioning that the latter experiment, performed in Hall C at Jefferson Lab [26], produced data that cannot be described by current theoretical models of the D(e,e'p)n reaction and may indicate an onset of non-nucleonic components in the deuteron at missing momenta above 750 MeV/c[27].

We now shift our focus to the kinematics dominated by FSI. As it was discussed in the introduction (I), our goal is to verify whether isolating the FSI will offer a possibility to probe the nucleon-nucleon scattering amplitude.
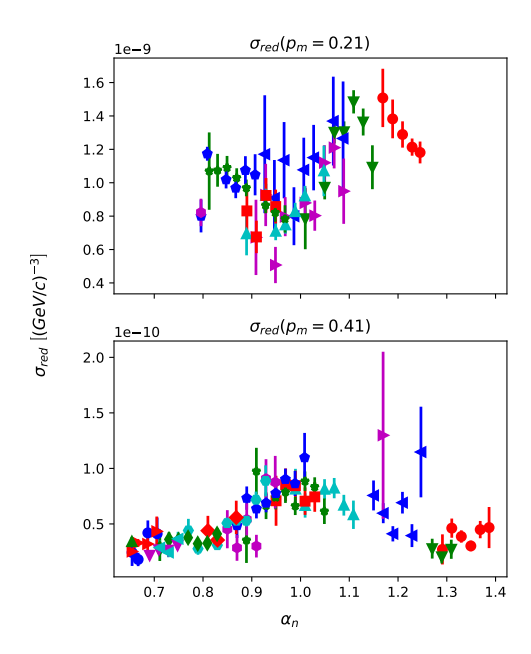

FIG. 6. Experimental reduced cross sections as a function of α_n. Top panel $p_m = 0.21$ GeV/c, bottom panel $p_m = 0.41$ GeV/c. As in Fig. 5, the different color and symbol combinations correspond to the different contributing spectrometer settings.

For this, according to Sec. III one needs to isolate the double-scattering contribution to the reaction (1). As a first step in this direction we re-analyzed the Hall A data at Q^2-values of 2.1 and 3.5 (GeV/c)^2 for missing momenta $p_m = 0.2, 0.4$ and 0.5 GeV/c with recoil neutrons produced centered around the $\phi_{nq} = 0^0$ plane. Since we found that the $p_m = 0.5$ GeV/c data are more sensitive to the deuteron wave function, we focus this re-scattering analysis on the missing momentum settings $p_m = 0.2$ and 0.4 GeV/c. The data at $Q^2 = 2.1 \pm 0.25$(GeV/c)^2 (here ± 0.25 indicates the Q^2 bin width) were taken at an average beam energy of 4.703 GeV and the ones at $Q^2 = 3.5 \pm 0.25$(GeV/c)^2 were taken at an average beam energy of 5.008 GeV. The analysis of the two Q^2 data-

sets, proceeded almost identical to the analysis described in Ref. [23]. The coincidence efficiencies were determined from ^{1}H(e,e′p) measurements and found to be $97 \pm 5.5\%$ and $96 \pm 2\%$, for the $Q^2 = 2.1$ and $Q^2 = 3.5$ (GeV/c)^2 data-sets, respectively. For every kinematic bin the systematic error due to uncertainties in the measured kinematic variables was estimated and added in quadrature to the statistical error. An additional estimated global systematic error of 4.0% was added in quadrature to take into account uncertainties in beam charge measurements, detector efficiencies, target thickness determination, target boiling corrections and the nucleon form factor data.
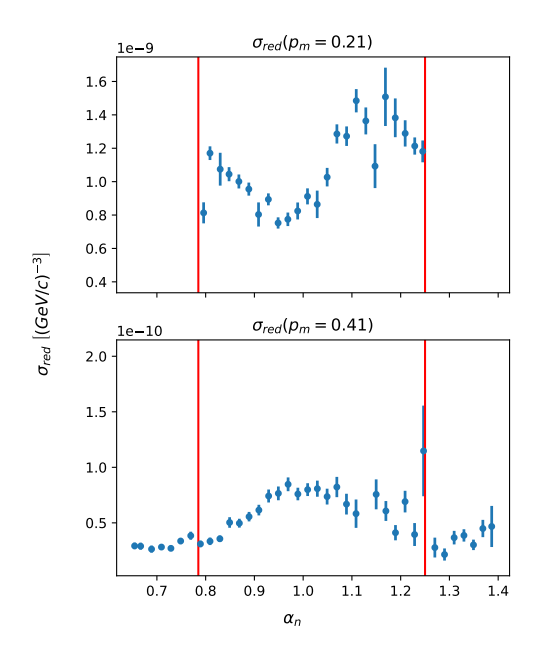

FIG. 7. Average experimental reduced cross sections as a function of α_n. Top panel $p_m = 0.21$ GeV/c, bottom panel $p_m = 0.41$ GeV/c. The red vertical lines indicate the region of overlapping α_n values which will be used in the analysis described below.

We determined absolute cross sections as a function of missing momentum and neutron light-front momentum fraction:

$$\alpha_n = \frac{E_n - p_{n,z}}{M_d/2} \tag{20}$$

using a missing momentum bin size of $\Delta p_m = \pm 0.01$ GeV/c and a momentum fraction bin size of $\Delta \alpha_n = \pm 0.01$. In the above equation $p_{n,z}$ is the component of the recoil neutron momentum in the **q** direction. The rationale for choosing the neutron's light cone momentum fraction as a kinematic parameter was discussed in Sec. III.

As an example, Fig. 5 shows the measured cross sections for missing momentum values of $p_m = 0.21$ and 0.41 GeV/c. The data are shown in groups of different color and symbol combinations. Data points with the same color and symbol belong to the same spectrometer

setting. The measured cross sections for a given value of α_n from different spectrometer settings differ considerably which is due to slightly different kinematic settings (electron scattering angle, proton direction etc.) that result in the same α_n and p_m bin and it is quite difficult to observe an emerging structure from these cross sections. This situation changes when one evaluates the reduced cross sections defined as follows:

$$\sigma_{red} = \frac{\sigma_{exp}}{k\sigma_{ep}f_{rec}} \tag{21}$$

where k is a kinematic factor, σ_{ep} the calculated off-shell e-p cross section and f_{rec} a recoil factor. The factors are chosen such that σ_{red} would correspond to the momentum distribution if there were no FSI and no other processes such as meson exchange currents and isobar configuration contributing to the cross section that destroy the relation $\vec{p}_i = -\vec{p}_{miss}$, where $\vec{p}_i$ is the initial momentum of the bound nucleon.

The resulting reduced cross sections as shown in Fig. 6 significantly diminish many of the cross section variations in a given $\alpha_n - p_m$ bin. The data-points of the different spectrometer settings are now statistically overlapping and a clearer pictures emerges.

Within PWIA, for constant missing momentum the observed reduced cross section should be independent of α_n and observed deviations at considered Q^2 are due to (non-PWIA) processes of Fig.(1) (b),(c) and (d). As Fig.6 shows the observed reduced cross sections are not independent of α_n. Moreover they show pattern similar to Fig.3; a reduction abound $\alpha_n \approx 0.95 - 1.0$ for $p_m = 0.21$ GeV/c and a sizable enhancement at the same α_n value for $p_m = 0.41$ GeV/c. As a next step we calculated the weighed mean of all spectrometer contributions for each α_n-bin and for each p_m value. The result is shown in Fig. 7. The vertical red lines indicate the range of common α_n values for the two missing momentum settings allowing for a comparative study of double-scattering in the D(e,e′p)n reaction discussed in the following section. The variations of the reduced cross sections for the two different missing momentum settings are now very clear, allowing to identify the domain of maximal FSI.

V. COMPARISON OF THEORY WITH EXPERIMENT

As above experimental analysis shows that data clearly indicate the enhanced FSI contribution at $\alpha_n = \alpha_r \approx 1$ and demonstrate the pattern predicted in Fig.3. In Ref.[23] the first theoretical comparison was focused on isolating kinematics most sensitive to the genuine deuteron structure, by minimizing FSI contribution. As Fig.8 shows, indeed such kinematics were found at $\theta_{nq} \leq 40^0$ in which the large sensitivity to the deuteron wave function was observed. The same comparison (right panel of Fig.8) also demonstrates the enhanced role of
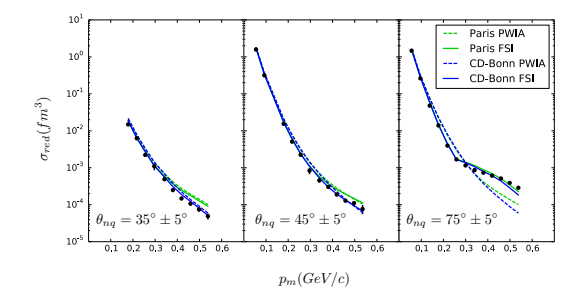
FIG. 8. Comparision of GEA calculation with reduced experimental cross sections

final state interactions at $\theta_{nq} \approx 75^0$. As the latter shows starting at $p_r = p_m \geq 400$ MeV/c the cross section is almost all due to rescattering contribution as it was discussed in Sec.III.

We focus now on kinematics dominated by final state interaction. In Fig.9 one observes that the data unambiguously identify the kinematics dominated by the interference (at $p_R = p_m \approx 200$ MeV/c) and double scattering (at $p_r = p_m \approx 400$ MeV/c) terms in Eq.(18) (compare with Fig.3). The data also confirms that the maximum of FSI takes place at $\alpha_n \approx 1$.

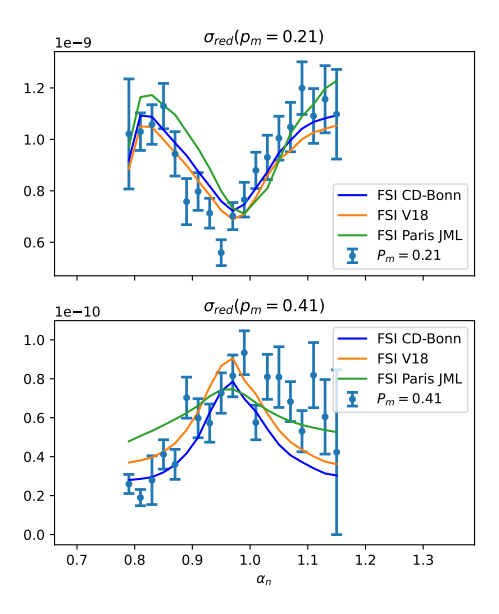FIG. 9. Comparison of theoretical calculations with reduced experimental cross sections at $p_m = 201$ MeV/c and 401 MeV/c for the range of α_n.

It is worth noting that the underestimation of calculations at $\alpha_n > 1.1$ is most probably due to intermediate Δ-isobar production since it corresponds to the kinematics close to the threshold of Δ production in the intermediate state. The calculations presented in Fig.9 do not include intermediate Δ -isobar contribution (similar to

Fig.1 (d)).

As the lower panel of Fig.9 shows it has a clear signature of maximal double scattering contribution, at $p_m = 400$ MeV/c, similar to Fig.3 (b) and (d). Thus we attempt to check the validity of the statement that the double scattering term is sensitive to the shape of $\mid f_{pn} \mid^2$ as it was presented in Fig.4. For this we evaluated the experimental ratio R of Eq.(19) by dividing the experimental cross sections by PWIA calculations at $p_r = p_m = 400$ MeV/C averaged over $\alpha_n = 1 \pm 0.1$, measured at $Q^2 = 2$ and 3.5 $(\text{GeV/c})^2$ corresponding to the total invariant energy of $s = 5.8$ and 7.9 GeV^2 respectively. In theoretical calculations we choose the CD-Bonn wave function of the deuteron which gave an overall best description of the data for all kinematics of the experiments.
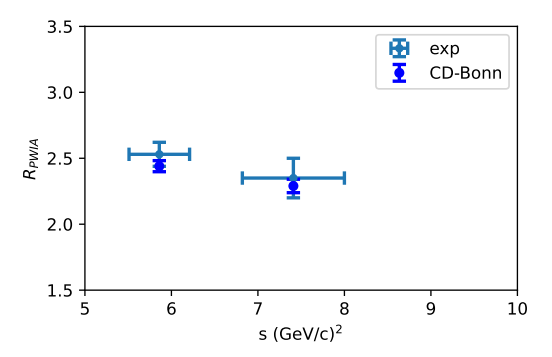

FIG. 10. Comparison of theoretical calculations with reduced experimental cross section ratios at $p_m = 410$ MeV/c for the range of $\alpha_n = 1 \pm 0.1$..

As Fig.10 shows despite s being relatively small that ChEx-FSI neglected in Fig.4 is not negligible, the first such comparison indicates that the data reproduce the shape of the $\mid f_{pn} \mid^2$ amplitude that enters in FSI. Note that the ratio in Fig.10 for both the experiment and theory has been determined by fitting a parabola to the peak regions ($\alpha_n = 1 \pm 0.1$) and the respective maxima have been determined from the fitting parameters resulting in error bars for experimental data as well as for theoretical calculations.

Finally, in Fig.11 we present α_n dependence of the ratio of reduced cross sections measured at double scattering ($p_m \approx 400$ MeV/c) and interference ($p_m \approx 200$ MeV/c) kinematics.

$$R_\sigma = \frac{\sigma_{red}(p_m = 0.41)}{\sigma_{red}(p_m = 0.21)}. \qquad (22)$$

The rationale of constructing such a ratio (see e.g. Ref.[28]) follows from the fact that it has maximal sensitivity to the features of the f_{pn} amplitude, since any modification of the latter will have opposite effects for cross sections measured at $p_m \approx 400$ MeV/c and $p_m \approx 200$ MeV/c. For example if the rescattering amplitude decreases with Q^2 it will diminish the double scattering dominated cross section that enters in the numerator
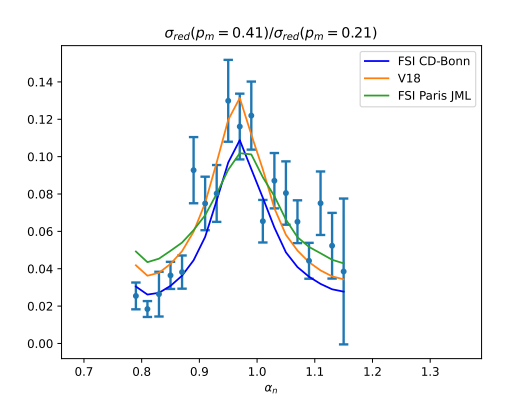
FIG. 11. The α_n dependence of R_σ, defined in Eq.(22).

and increase the interference term dominated cross section that enters in the numerator of ratio R_σ (22).

As Fig.11 shows theoretical calculations describe reasonably well the first experimental evaluation of ratio R_σ. It is interesting that as the figure shows the above discussed intermediate Δ-isobar contribution which is not included in the calculations largely cancels out in the ratio. This can be understood from the fact that the amplitude of intermediate Δ-isobar contribution is predominantly real which does not interfere with the PWIA term, thus having same effects in both numerator and denominator of ratio, R_σ.

VI. CONCLUSION AND OUTLOOK

We presented the first analysis of the high Q^2 electro-disintegration of the deuteron in double scattering kinematics. Our main goal was to check the conjecture that the double scattering subprocess can be unambiguously identified in the exclusive deuteron electrodisintegration reaction and its energy (or Q^2) dependence reflects the energy dependence of pn scattering amplitude. We took advantage of the fact that the first moderately high Q^2 experiments are performed in the invariant energy range in which pn scattering amplitude has noticeable energy dependence (Fig.2)) thus providing sensitive test for the double scattering method of probing the pn-amplitude.

The comparison with theory shows a reasonable agreement with the existing data confirming the sensitivity of double scattering processes to the energy dependence of the pn-scattering amplitude (Fig.10). This result indicates that the achieved accuracy in the description of the moderately high Q^2 data in the nucleonic basis allows us to extend the considered reactions into a higher energy domain in which the onset of QCD degrees of freedom is expected to modify rescattering processes due to the dominance of small size color neutral configurations in the wave function of produced baryons at high Q^2.

Currently, the double scattering subprocess for the reaction (1) is planned to be measured for Q^2 as large as 14 $(\text{GeV/c})^2$[11] and it can significantly advance our understanding of the dynamics of the pn scattering amplitude in the deuteron at large Q^2.

The deuteron disintegration can be extended also to deep inelastic kinematics for $d(e, e', N_r)X$ reactions in which case the detection of the spectator nucleon N_r can be used to probe the reinteraction of the product of $\gamma^* N \to X$ scattering off the spectator nucleon[29]. Such processes can be effective also for studying hadronization dynamics by isolating the rescattering of a hadron, h produced in $\gamma^* N \to h + X$ reaction off the spectator nucleon, N_r[30]. The consideration of these processes in Electron-Ion Collider kinematics can significantly increase the effectiveness of these reactions allowing the clear separation of current and target fragmentation regions.

[1] K. Adcox *et al.* (PHENIX), Nucl. Phys. A **757**, 184 (2005), arXiv:nucl-ex/0410003.

[2] G. Aad *et al.* (ATLAS), JINST **3**, S08003 (2008).

[3] S. J. Brodsky and A. H. Mueller, Phys. Lett. B **206**, 685 (1988).

[4] K. Geiger, Phys. Rev. D **47**, 133 (1993).

[5] M. He and R. Rapp, Phys. Rev. Lett. **124**, 042301 (2020), arXiv:1905.09216 [nucl-th].

[6] A. Airapetian *et al.* (HERMES), Nucl. Phys. B **780**, 1 (2007), arXiv:0704.3270 [hep-ex].

[7] B. Z. Kopeliovich, J. Nemchik, E. Predazzi, and A. Hayashigaki, Nucl. Phys. A **740**, 211 (2004), arXiv:hep-ph/0311220.

[8] L. L. Frankfurt, W. R. Greenberg, G. A. Miller, M. M. Sargsian, and M. I. Strikman, Z. Phys. A **352**, 97 (1995), arXiv:nucl-th/9501009.

[9] L. L. Frankfurt, W. R. Greenberg, G. A. Miller, M. M. Sargsian, and M. I. Strikman, Phys. Lett. B **369**, 201 (1996), arXiv:nucl-th/9412033.

[10] J.-M. Laget, in *Workshop on Color Transparency (CT 97)* (1998) pp. 121–129.

[11] H. Szumila-Vance, D. Higinbotham, S. Li, J. Rittenhouse West, and C. Yero (spokespersons), Jefferson Lab Proposal **PR12-23-010** (2023).

[12] M. M. Sargsian, Int. J. Mod. Phys. E **10**, 405 (2001), arXiv:nucl-th/0110053.

[13] S. Jeschonnek and J. W. Van Orden, Phys. Rev. C **78**, 014007 (2008), arXiv:0805.3115 [nucl-th].

[14] W. P. Ford, S. Jeschonnek, and J. W. Van Orden, Phys. Rev. C **87**, 054006 (2013), arXiv:1304.0647 [nucl-th].

[15] C. Ciofi degli Atti and L. P. Kaptari, Phys. Rev. C **71**, 024005 (2005), arXiv:nucl-th/0407024.

[16] J. M. Laget, Phys. Lett. B **609**, 49 (2005), arXiv:nucl-th/0407072.

[17] M. M. Sargsian, Phys. Rev. C **82**, 014612 (2010), arXiv:0910.2016 [nucl-th].

[18] W. Boeglin and M. Sargsian, Int. J. Mod. Phys. E **24**, 1530003 (2015), arXiv:1501.05377 [nucl-ex].

[19] V. N. Gribov, Zh. Eksp. Teor. Fiz. **57**, 1306 (1969).

[20] L. Bertuchi, IL Nuovo Cimento A **11**, 45 (1972).

[21] L. L. Frankfurt, M. M. Sargsian, and M. I. Strikman, Phys. Rev. C **56**, 1124 (1997), arXiv:nucl-th/9603018.

[22] R. L. Workman *et al.* (Particle Data Group), PTEP **2022**, 083C01 (2022).

[23] W. U. Boeglin *et al.* (For the Hall A Collaboration), Phys. Rev. Lett. **107**, 262501 (2011).

[24] K. Egiyan *et al.* (CLAS Collaboration), Phys.Rev.Lett. **98**, 262502 (2007), arXiv:nucl-ex/0701013 [nucl-ex].

[25] H. Khanal, *Experimental Deuteron Momentum Distributions with Reduced Final State Interactions*, PhD dissertation, Florida International University (2014).

[26] C. Yero *et al.* (Hall C), Phys. Rev. Lett. **125**, 262501 (2020), arXiv:2008.08058 [nucl-ex].

[27] M. M. Sargsian and F. Vera, Phys. Rev. Lett. **130**, 112502 (2023), arXiv:2208.00501 [nucl-th].

[28] S. Li, C. Yero, J. R. West, C. Bennett, W. Cosyn, D. Higinbotham, M. Sargsian, and H. Szumila-Vance, MDPI Physics **4**, 1426 (2022), arXiv:2209.14400 [nucl-ex].

[29] W. Cosyn and M. Sargsian, Phys. Rev. C **84**, 014601 (2011), arXiv:1012.0293 [nucl-th].

[30] W. Cosyn and M. Sargsian, Int. J. Mod. Phys. E **26**, 1730004 (2017), arXiv:1704.06117 [nucl-th].